Elasticity of (Mg,Fe)O Through the Spin Transition of Iron in the Lower Mantle

J. C. Crowhurst, *et al.*

Science **319**, 451 (2008);
DOI: 10.1126/science.1149606

Science (print ISSN 0036-8075; online ISSN 1095-9203) is published weekly, except the last week in December, by the American Association for the Advancement of Science, 1200 New York Avenue NW, Washington, DC 20005.

Elasticity of (Mg,Fe)O Through the Spin Transition of Iron in the Lower Mantle

J. C. Crowhurst,[1]* J. M. Brown,[2] A. F. Goncharov,[3] S. D. Jacobsen[4]

Changes in the electronic configuration of iron at high pressures toward a spin-paired state within host minerals ferropericlase and silicate perovskite may directly influence the seismic velocity structure of Earth's lower mantle. We measured the complete elastic tensor of ferropericlase, $(Mg_{1-x},Fe_x)O$ ($x = 0.06$), through the spin transition of iron, whereupon the elastic moduli exhibited up to 25% softening over an extended pressure range from 40 to 60 gigapascals. These results are fully consistent with a simple thermodynamic description of the transition. Examination of previous compression data shows that the magnitude of softening increases with iron content up to at least $x = 0.20$. Although the spin transition in (Mg,Fe)O is too broad to produce an abrupt seismic discontinuity in the lower mantle, the transition will produce a correlated negative anomaly for both compressional and shear velocities that extends throughout most, if not all, of the lower mantle.

Knowledge of the physical properties of various transition-metal oxides is crucial to interpreting the seismic structure of Earth in terms of mineralogical and compositional variations. Iron is the most abundant transition metal in Earth. In the lower mantle (which extends from the 660-km discontinuity to the core-mantle boundary at a depth of 2900 km), it is hosted by ferropericlase [(Mg,Fe)O] and silicate perovskite [$(Mg,Fe)SiO_3$]. Mineralogical models of the lower mantle indicate that ferropericlase constitutes 10 to 20% of this region by volume (*1*–*3*), which partitions iron with silicate perovskite in fractions depending on both temperature and depth (*4*–*9*). Recently, the important question of spin-pairing transitions of iron from high-spin (HS) to low-spin (LS) states in ferropericlase (*7*, *10*–*17*), affecting the lower mantle's density and seismic wave velocities, has been recognized (*11*, *12*). Because knowledge of this deep and inaccessible region is derived largely from seismic data, it is essential to determine the influence of the spin transition on elastic wave velocities at lower-mantle pressures.

In ferropericlase, the spin transition occurs without change from the NaCl crystal structure or distortion of its cubic symmetry (*11*). Nevertheless, as we show, the spin-pairing transition interval is accompanied by softening of all the single-crystal elastic moduli (c_{11}, c_{12}, and c_{44}) by up to 25% between 40 and 50 GPa. Consequent recovery of the elastic moduli between 50 and 60 GPa brings velocities close to those extrapolated from the low-pressure HS state. The elastic behavior is continuous and consistent with a macroscopic thermodynamic description of the transition, which is inherently non–first order. The observed anomalies in elastic properties of this material with ~6% iron represent a minimum effect, which would be enhanced in compositions with more iron and in the range of expected lower-mantle compositions of 10 to 15% iron.

Single crystals of $(Mg_{0.94},Fe_{0.06})O$ were loaded into the cavity of a diamond anvil cell with an argon pressure-transmitting medium. Impulsive stimulated scattering was used to measure body and interfacial acoustic velocities over a 60° range in a (100)-type plane at increments of 10° (*18*).

At lower pressures, the data (circles in Fig. 1) are in agreement with those calculated on the basis of an extrapolation of a linear fit to the elastic properties determined by Jackson *et al*. (*19*) to 20 GPa (solid lines). However, near 40 GPa, all velocities begin to decrease relative to the extrapolation and reach minima between 47 and 50 GPa. Velocities then begin to increase again and approach those of the extrapolation above 60 GPa.

All three elastic constants (Fig. 2) inferred from the acoustic wave velocities [supporting online material (SOM) text] exhibit normal behavior below 40 GPa. In the pressure regime between 40 and 60 GPa, all the c_{ij} show substantial softening and then consequent recovery relative to the linear extrapolations after passing through minima at about 48 GPa. The anisotropy parameter A [i.e., the difference between the shear moduli $c'=(c_{11}-c_{12})/2$ and c_{44}], which is equal to zero for isotropic solids, is negative at low pressure, passes through zero near 20 GPa, and continues on a smooth positive trend at higher pressure. Unlike the individual constants, no anomalous dependence is apparent in the 40- to 60-GPa regime (*20*).

The spin transition in ferropericlase is associated with a decrease in volume (*11*) that is dependent on iron concentration (x) [e.g., (*15*, *16*, *21*)]. A heuristic explanation, based on the geometry of 3*d* electronic orbitals, rationalizes a coupling of the spin transition with acoustic wave velocities. The five 3*d* electronic states for iron are divided into two e_g orbitals (spatially directed toward the neighboring oxygen anions) and three t_{2g} orbitals (spatially oriented between the neighboring oxygen anions). Occupation of the e_g orbitals (giving rise to higher electron density along the iron-oxygen bond) tends to expand the lattice. An additional lattice distortion breaks cubic local symmetry to lift the degeneracy of the e_g states (the Jahn-Teller effect). In HS ferropericlase, each

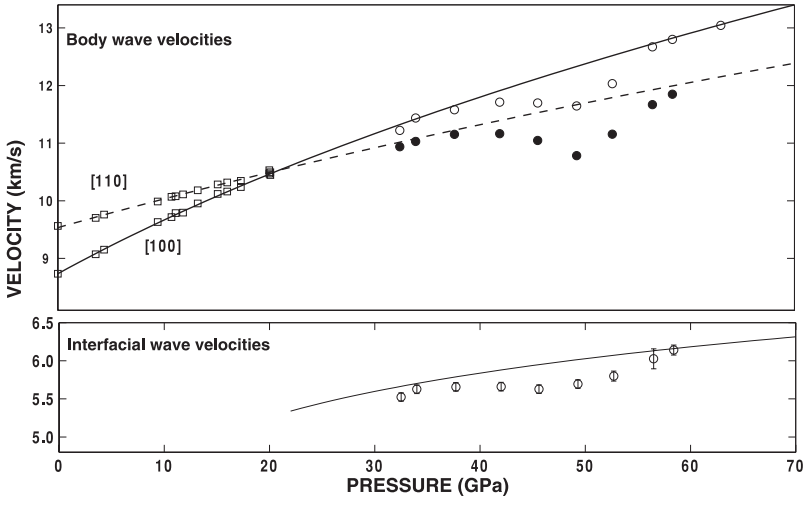

Fig. 1. Acoustic wave velocities as a function of pressure for propagation in the (001) plane of single-crystal $(Mg_{0.94},Fe_{0.06})O$ in an argon pressure-transmitting medium. Circles indicate present data acquired by impulsive stimulated scattering. Uncertainties are given by ± 2σ, where σ is the formal SE. Squares indicate data obtained by Jackson *et al*. via Brillouin scattering (*19*). Lines are calculated velocities based on linear extrapolations of the elastic moduli obtained by Jackson *et al*. (*19*). (**Top**) Body wave velocities. Solid circles and open circles are data for propagation along [110] and [100], respectively. (**Bottom**) Velocities of the wave that propagates at the interface between the sample and the pressure-transmitting medium. The interfacial wave has no dependence on direction under these conditions.

[1]Chemistry, Materials, and Life Sciences Directorate, Lawrence Livermore National Laboratory (LLNL), Livermore, CA 94550, USA. [2]Earth and Space Sciences, University of Washington, Seattle, WA 98195, USA. [3]Geophysical Laboratory, Carnegie Institution of Washington, Washington, DC 20015, USA. [4]Department of Earth and Planetary Sciences, Northwestern University, Evanston, IL 60208, USA.

*To whom correspondence should be addressed. E-mail: crowhurst1@llnl.gov

e_g state is occupied by an unpaired electron, giving rise to antiferromagnetic coupling, an expanded lattice, and noncubic local symmetry. In the LS state, all six 3*d* electrons are contained in the three t_{2g} orbitals. Transition to the LS state is accompanied by a decrease in volume and reduction or altering of the lattice distortion. HS and LS states coexist with a statistical distribution that is dependent on pressure *P* and temperature *T*. The LS state is not favored at low pressure as a result of the exchange energy involved in pairing of electrons in the otherwise lower-energy t_{2g} orbitals. An expression for the fraction of iron cations in the LS state (*n*) can be derived through minimization of the Gibbs energy with respect to *n* (*15*). It is dependent on the enthalpy difference ($\Delta H = \Delta E + P\Delta V$, where ΔV and ΔE are the change in volume and the change in internal energy associated with the transition, respectively) between the two states

$$n = \frac{1}{1 + m(2s+1)e^{\frac{\Delta H}{kTs}}} \qquad (1)$$

where *m* and *s* are the electronic degeneracy and iron spin quantum number, respectively, of the HS state, and *k* is Boltzmann's constant. Increasing pressure drives the system into the LS configuration as a result of the $P\Delta V$ energy associated with the transition (*16*). However, at finite temperature, a consequence of Eq. 1 is that the transition is non–first order. Acoustic waves, as agents of both dilatational and shear strains, couple to the spin transition if it and the consequent changes in size and geometry are fast as compared with the acoustic period. In the region of transition, a positive increment of stress will drive the system toward the LS state. In turn, this causes an increment of strain in excess of the normal elastic behavior. A softening of the associated elastic moduli thus occurs. The volume and geometric changes discussed above are at least qualitatively sufficient to account for softening of both the compressional and shear moduli.

Lin *et al.* (*11*) reported compression data to 135 GPa for ferropericlase with 17% iron in a neon pressure-transmitting medium. These data (Fig. 3) clearly show three regimes: HS behavior below 40 GPa, LS behavior above 60 GPa, and a transition regime between 40 and 60 GPa. Fourth-order finite-strain equations-of-state fits are plotted in the figure as dashed lines. As predicted by ab initio calculations (*15*, *16*), HS and LS iron have similar equations of state that are simply displaced by a ΔV of transition. A curve (depicted as the thick solid line in Fig. 3) fitting all compression data was constructed on the basis of Eq. 1 and linear volume mixing. The ab initio prediction is depicted as the thin solid line. Because ΔV is determined by the equations of state for the two spin states, a linear dependence of ΔE on pressure was adjusted to fit the compression data. The change in ΔH that was responsible for the HS-to-LS transition is principally associated with the increasingly negative contribution from $P\Delta V$ (Fig. 4). ΔE changes only modestly over this pressure regime.

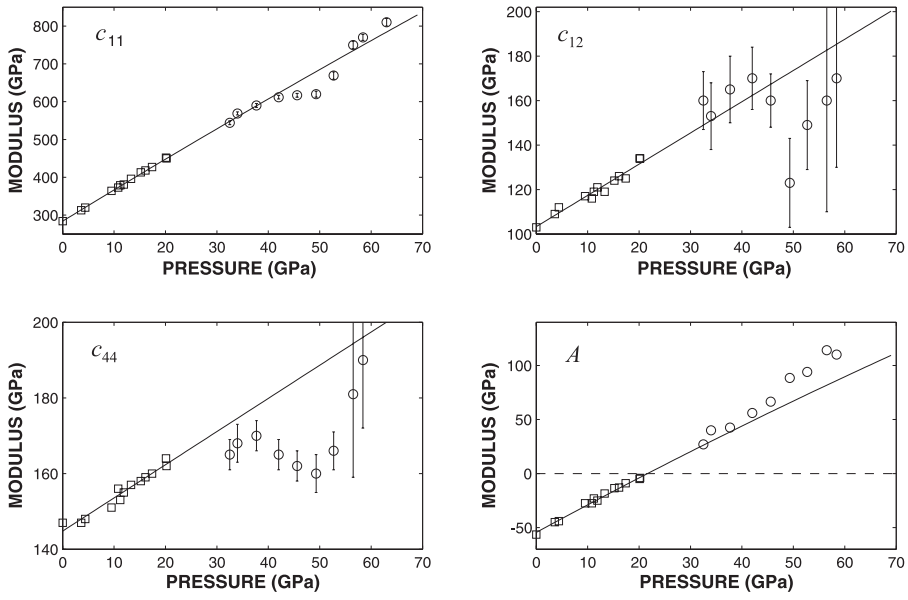

Fig. 2. Measured pressure dependence of the elastic moduli c_{ij} and anisotropy factor $A = (c_{11} - c_{12})/2 - c_{44}$. Circles indicate the present data, and squares are data of Jackson *et al.* (*19*). Lines are linear fits to the latter data. Error bars indicate two SEs obtained from fits to the measured velocities.

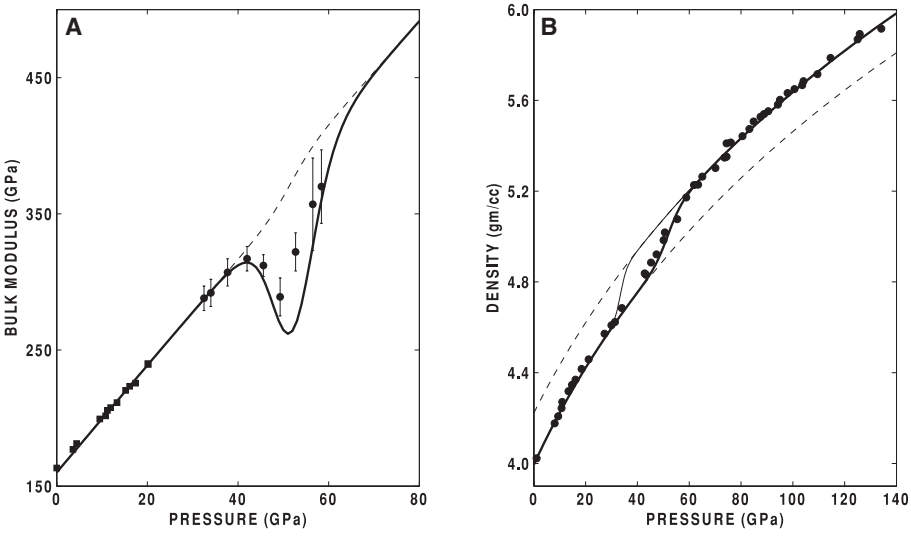

Fig. 3. (**A**) Bulk modulus versus pressure. Circles indicate present data calculated on the basis of the c_{ij} shown in Fig. 2. Squares are values calculated on the basis of the data of Jackson *et al.* (*19*). The solid line is based on a thermodynamic description of the HS-to-LS transition with parameters scaled from those that fit the compression data of Lin *et al.* (*11*). The dashed line is the average of separate equations of state for the HS and LS phases [see (B)]. Error bars indicate two SEs obtained from fits to the measured velocities. (**B**) Experimental data of Lin *et al.* (*11*) showing density of $(Mg_{0.83},Fe_{0.17})O$ versus pressure. The dashed lines represent equations-of-state (fourth-order Eulerian finite-strain) fits (*22*) to the HS (low pressure) and LS phases. The thick solid line is a fit to the data based on Eq. 1. The thin solid line is the first-principles theoretical prediction of Tsuchiya *et al.* (*15*).

In the dilute limit (noninteracting iron sites), thermophysical properties should scale linearly with iron concentration (*15*). We therefore scale terms in Eq. 1 and Fig. 4 from the $x = 17\%$ material investigated by Lin *et al.* (*11*) to our sample with $x = 6\%$. The agreement in the pressure regime of transition and degree of modulus softening suggests that the thermodynamic description is reasonable (Fig. 3). Using the same approach, we have also compared our data to the compression data obtained by Fei *et al.* (*21*) for material with $x = 20\%$ (fig. S2) in an annealed NaCl pressure-transmitting medium. Although the latter data suggest a minimum in the bulk modulus at a lower pressure of about 39 GPa, the observation of the softening, its magnitude, and the extent of pressure over which it occurs are entirely consistent with our results.

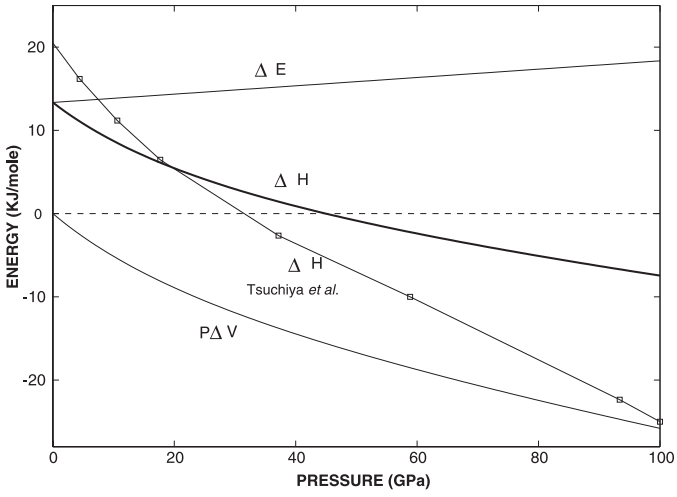

Fig. 4. HS-to-LS transition enthalpy, $\Delta H = \Delta E + P\Delta V$, and component terms, ΔE and $P\Delta V$. The thick solid line showing the enthalpy was obtained from the data of Lin *et al*. (*11*) (see text). It is a sum of the individual components shown. The line with squares is the result of a first-principles calculation by Tsuchiya *et al*. (*15*).

We have measured the elastic tensor of $(Mg_{0.94},Fe_{0.06})O$ through the pressure-induced HS-to-LS transition. We find that there is an extensive range of pressure over which all the c_{ij} exhibit an anomalous but smooth softening. By reinterpreting previously published compression data of materials with much higher iron concentrations (more representative of the lower mantle), we show that similar but even more pronounced behavior is exhibited by at least the bulk modulus. The current data show that, even at room temperature, the HS-to-LS transition in (Mg,Fe)O is not expected to result in a sudden increase in seismic velocities at any depth. Although this finding is inconsistent with the conclusions of (*11*), it is qualitatively consistent with the results of the more recent x-ray emission experiment carried out at simultaneous high pressure and temperature by Lin *et al*. (*17*), who noted that the spin transition takes place over an extended range of pressure and temperature. On the basis of our room-temperature results, this range extends from 1000 to 1500 km. At elevated temperatures and on the basis of Eq. 1, this range increases to include most or all of the lower mantle and results in a decrease in compressional and shear velocities of a few percent.

References and Notes

1. E. Ito, E. Takahashi, *J. Geophys. Res.* **94**, 10637 (1989).
2. T. Irifune *et al*., *Science* **279**, 1698 (1998).
3. C. R. Bina, *Rev. Mineral. Geochem.* **37**, 205 (1998).
4. S. E. Kesson, J. D. Fitz Gerald, H. St. C. O'Neill, J. M. G. Shelley, *Phys. Earth Planet. Inter.* **131**, 295 (2002).
5. Y. Fei, *Rev. Mineral. Geochem.* **37**, 343 (1998).
6. D. Andrault, *J. Geophys. Res.* **106**, 2079 (2001).
7. J. Badro *et al*., *Science* **300**, 789 (2003).
8. M. Murakami, K. Hirose, N. Sata, Y. Ohishi, *Geophys. Res. Lett.* **32**, L03304 (2005).
9. Y. Kobayashi *et al*., *Geophys. Res. Lett.* **32**, L19301 (2005).
10. S. Speziale *et al*., *Proc. Natl. Acad. Sci. U.S.A.* **102**, 17918 (2005).
11. J. F. Lin *et al*., *Nature* **436**, 377 (2005).
12. J. F. Lin *et al*., *Geophys. Res. Lett.* **33**, L22304 (2006).
13. A. F. Goncharov, V. V. Stuzhkin, S. D. Jacobsen, *Science* **312**, 1205 (2006).
14. W. Sturhahn, J. M. Jackson, J. F. Lin, *Geophys. Res. Lett.* **32**, L12307 (2005).
15. T. Tsuchiya, R. M. Wentzcovitch, C. R. S. da Silva, S. de Gironcoli, *Phys. Rev. Lett.* **96**, 198501 (2006).
16. H. Persson, A. Bengtson, G. Ceder, D. Morgan, *Geophys. Res. Lett.* **33**, L16306 (2006).
17. J. F. Lin *et al*., *Science* **317**, 1740 (2007).
18. Materials and methods are available as supporting material on *Science* Online.
19. J. M. Jackson *et al*., *J. Geophys. Res.* **111**, 09203 (2006).
20. Acoustic velocities and moduli are tabulated in tables S1 and S2. Figure S1 presents the inferred aggregate shear modulus as a function of pressure.
21. Y. Fei *et al*., *Geophys. Res. Lett.* **34**, L17307 (2007).
22. Parameters for the HS phase are $K_0 = 158$ GPa, $K' = 4.0$, and $K'' = 0$, with $\rho_0 = 3.994$ g cm^{-3} (where K_0, K', K'', and ρ_0 are the bulk modulus, the first and second derivatives of the bulk modulus, and the density at zero pressure). For the LS phase, they are $K_0 = 185$ GPa, $K' = 3.90$, and $K'' = 0$, with $\rho_0 = 4.221$ g cm^{-3}.

23. J.C.C. acknowledges W. Sturhahn and M. Armstrong for useful discussion. J.M.B. acknowledges support from NSF EAR 0106683. A.F.G. acknowledges support from the U.S. Department of Energy (DOE)/National Nuclear Security Agency through the Carnegie/DOE Alliance Center, NSF, and the W. M. Keck Foundation, and acknowledges V. Struzhkin for useful comments and discussions. S.D.J. acknowledges support from NSF EAR 0721449 and acknowledges J. F. Lin, S. J. Mackwell, and C. A. McCammon for discussions and help with sample synthesis and characterization. We thank two anonymous reviewers for constructive criticism and suggestions. This work was performed under the auspices of the DOE by the University of California, LLNL under contract no. W-7405-Eng-48. The project 06-SI-005 was funded by the Laboratory Directed Research and Development Program at LLNL.

Supporting Online Material

www.sciencemag.org/cgi/content/full/319/5862/451/DC1
Materials and Methods
Figs. S1 and S2
Tables S1 and S2
References

22 August 2007; accepted 4 December 2007
10.1126/science.1149606

Enriched Pt-Re-Os Isotope Systematics in Plume Lavas Explained by Metasomatic Sulfides

Ambre Luguet,[1]*† D. Graham Pearson,[1] Geoff M. Nowell,[1] Scott T. Dreher,[1] Judith A. Coggon,[1] Zdislav V. Spetsius,[2] Stephen W. Parman[1]

To explain the elevated osmium isotope (^{186}Os-^{187}Os) signatures in oceanic basalts, the possibility of material flux from the metallic core into the crust has been invoked. This hypothesis conflicts with theoretical constraints on Earth's thermal and dynamic history. To test the veracity and uniqueness of elevated ^{186}Os-^{187}Os in tracing core-mantle exchange, we present highly siderophile element analyses of pyroxenites, eclogites plus their sulfides, and new $^{186}Os/^{188}Os$ measurements on pyroxenites and platinum-rich alloys. Modeling shows that involvement in the mantle source of either bulk pyroxenite or, more likely, metasomatic sulfides derived from either pyroxenite or peridotite melts can explain the ^{186}Os-^{187}Os signatures of oceanic basalts. This removes the requirement for core-mantle exchange and provides an effective mechanism for generating Os isotope diversity in basalt source regions.

The possibility of observing the chemical signature of core-mantle interaction in magmas erupted at Earth's surface is one of the most exciting prospects in mantle geochemistry. The observation of $^{186}Os/^{188}Os$-$^{187}Os/^{188}Os$ excesses in some plume-related lavas has recently been invoked as the strongest evidence of substantial mass exchange between the Earth's core and mantle (*1*–*5*). This hypothesis has considerable consequences for the evolution of the core, specifically requiring inner core crystallization early in Earth's history. This constraint on the inner core's crystallization age is in direct contradiction of recent models of terrestrial cooling (*6*, *7*) which predict ages of core crystallization as young as 1.5 billion years (Gy) old, too late then to generate the required ^{186}Os enrichment. Further objections to the core-mantle exchange model have come from the absence of $\varepsilon^{182}W$ anomalies in the same plume-related lavas (*8*) and from new high-pressure solid metal–liquid metal highly siderophile element (HSE) partition coefficients (*9*), which predict an outer core composition that is unable to generate elevated ^{186}Os and ^{187}Os, even over several billion years (Fig. 1). With the continued finding of $^{186}Os/^{188}Os$-$^{187}Os/^{188}Os$